10-2019

Quantifying the Effects of Hyperthermal Atomic Oxygen and Thermal Fatigue Environments on Carbon Nanotube Sheets for Space-Based Applications

Jacob W. Singleton

Gregory R. Cobb

Heath E. Misak
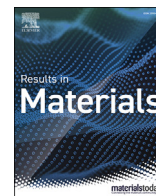
Ryan A. Kemnitz
Air Force Institute of Technology

Recommended Citation

Singleton, J. W., Cobb, G. R., Misak, H. E., & Kemnitz, R. A. (2019). Quantifying the Effects of Hyperthermal Atomic Oxygen and Thermal Fatigue Environments on Carbon Nanotube Sheets for Space-Based Applications. Results in Materials, 3(October), Art. No. 100034. https://doi.org/10.1016/j.rinma.2019.100034

Quantifying the effects of hyperthermal atomic oxygen and thermal fatigue environments on carbon nanotube sheets for space-based applications[★]

Jacob W. Singleton, Gregory R. Cobb [*], Heath E. Misak, Ryan A. Kemnitz

Air Force Institute of Technology, Department of Aeronautics and Astronautics, 2950 Hobson Way, Wright-Patterson AFB, OH, 45433-7765, USA

A B S T R A C T

The effects of atomic oxygen and thermal fatigue on two different types of carbon nanotube sheets were studied. One set was treated with nitric acid, while the other set was left untreated. Monotonic tensile tests were performed before and after exposure to determine the effects of either exposure type on the sheets' mechanical properties. Electrical conductivity and electromagnetic interference measurements were recorded to determine the effects of AO-exposure and thermal cycling on the sheets' electrical properties. Neither exposure type affected the sheets' specific strengths. Both exposure types increased the sheets' specific stiffnesses and decreased the sheets' strains at failure. The electrical conductivity of both sheets decreased due to the different exposure types, while the EMI shielding effectiveness was unaffected. Scanning electron microscopy was used to observe any changes in the sheets' surface morphologies, while energy-dispersive X-ray spectroscopy was used to determine the effects of AO on the sheets' chemical makeup.

1. Introduction

Carbon nanotubes (CNTs) are viewed as an ideal candidate for advanced applications due to their superb mechanical [1] and electrical [2] properties as well as their electromagnetic interference (EMI) shielding capability [3]. Their strong yet lightweight nature and ability to shield against EMI would be beneficial for space-based applications. Replacing existing materials with CNT-based materials would reduce the cost of a space launch, which is typically $20K USD per kilogram [4], or allow a greater payload at the same cost as a component built using traditional materials. Recent research has already indicated that they are a viable alternative to traditional copper cables and antennas [5,6], and they have already been implemented in the tubes and sandwich panels of the JUNO spacecraft [7]. CNT-based materials must be able to survive the harsh conditions found in low earth orbit (LEO). Therefore, further research must be performed in order to determine if they are suitable candidates for space-based applications.

LEO is a harsh environment for space structures with hazards that include atomic oxygen (AO), ultraviolet radiation, debris, and extreme temperature cycling. Composite materials exposed to this environment can exhibit reductions in their chemical, electrical, thermal, optical and mechanical properties as well as experience surface erosion [8]. AO is formed by photo dissociation of molecular oxygen in the upper atmosphere and constitutes approximately 80% of the LEO environment [8]. AO is found in LEO in densities of approximately 10^6-10^9 atoms cm^{-3} depending on such factors as the distance above the earth and the solar cycle, and a satellite travelling at 7 km s^{-1} could experience 10^{12}-10^{15} AO collisions cm^{-2} s^{-1} [9]. The AO particles collide with the satellite surface with a kinetic energy of about 5 eV [10]. This could be detrimental to components operating in LEO over a long period of time.

The effects of AO in LEO on organic materials have been well studied. A study by Shin et al. showed that the most detrimental effect of the space environment on organic polymers was material loss caused by AO erosion [11]. Han et al. reported a reduction in tensile strength and stiffness by 3.27% and 3.99% respectively for graphite/epoxy composites exposed to AO in simulated LEO as well as mass loss and surface erosion [12]. The use of CNTs in composites in LEO have also been studied. Moon et al. demonstrated that incorporating multi-walled CNTs into composites increased their baseline tensile strength and improve their resistance to the LEO environment [13]. However, these composites may not fully leverage the material properties of pure CNTs. Therefore, the effects of AO on products composed primarily of CNTs, such as CNT yarns, fibers,

---

[★] The views expressed in this article are those of the authors and do not reflect the official policy or position of the United States Air Force, Department of Defense, or the US Government.

[*] Corresponding author.
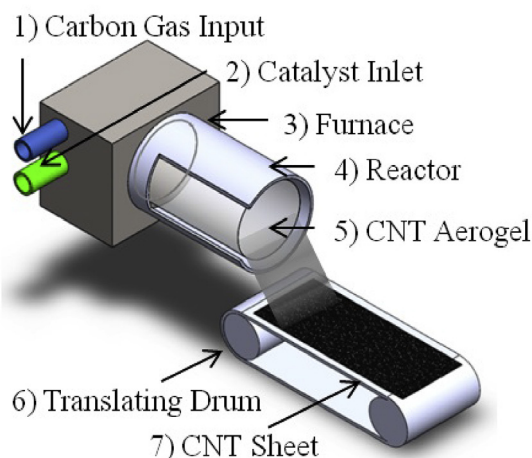*E-mail address:* gcobb@afit.edu (G.R. Cobb).

Fig. 1. Schematic of CNT sheet manufacturing process.

Table 1
Summary of the different specimen types.

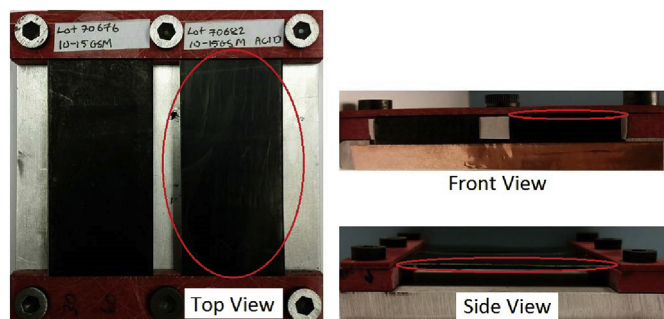| Specimen ID	Treatment	Exposure Type	Quantity Prepared
A-1	None	None	4
A-2	None	AO	4
A-3	None	Thermal	4
B-1	Acid	None	4
B-2	Acid	AO	4
B-3	Acid	Thermal	4

Fig. 2. Specimens prepared for exposure to AO and thermal fatigue. The specimen is circled.
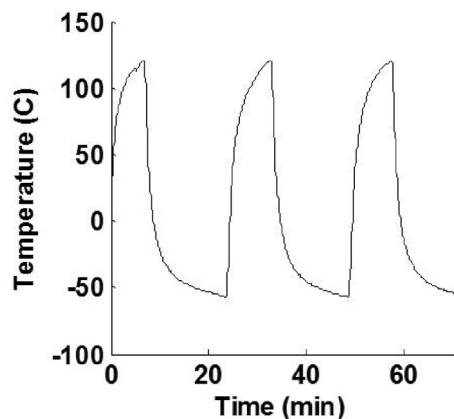

Fig. 3. First three temperature cycles used to study thermal fatigue. The temperature fluctuated at an average rate of ± 18 °C min^{-1}.
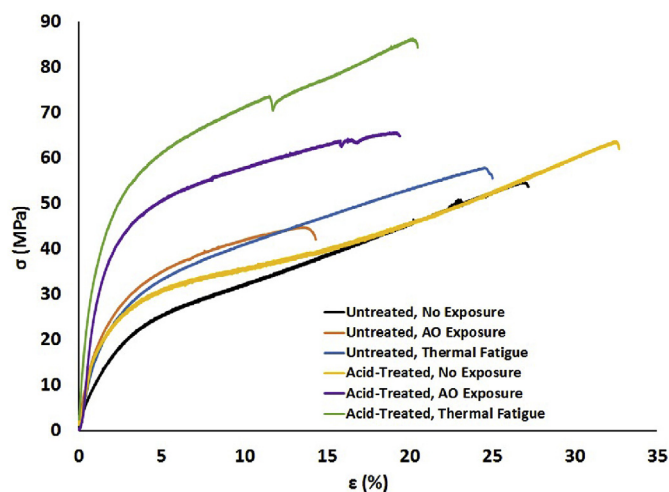

Fig. 4. Stress-strain data from a representative specimen from each set.

and sheets, must be studied as well. Previous AO-exposure studies have focused on CNT wires [14].

This study investigates the influence of AO exposure and thermal cycling on the mechanical and electrical properties of CNT sheets. These properties include the specific strength, specific stiffness, strain at failure, electrical conductivity, and EMI shielding. Stress-strain curves were generated for the specimens both pre- and post-exposure in order to determine any changes in the specimens' material properties. Changes in the CNT sheets' microstructure were analyzed using scanning electron microscopy (SEM) and energy-dispersive X-ray spectroscopy (EDS). This research expands on current knowledge of CNT survivability and serves as a reference for their suitability as components on space systems.

2. Materials and methodology

2.1. Material

The CNT sheets investigated in this study were Miralon sheets manufactured by Nanocomp Technologies, Inc. (Merrimack, New Hampshire, USA). The sheets were composed of multi-walled CNTs created via chemical vapor deposition with an iron catalyst. The nature of the sheets was verified with Raman spectroscopy in the authors' previous work [15]. They were deposited onto a translating drum and formed into a non-woven textile sheet as represented in Fig. 1. They were then condensed with acetone [16]. Two specimens sets were studied. The first set contained no further post-processing, while the second set was treated with nitric acid. Nitric acid has been shown to improve the electrical conductivity of CNT yarns [17], which could be beneficial for certain applications. The thicknesses of the sheets were measured at multiple locations on the specimens with a Rex MTG-DX2 Material Thickness Gauge (Rex Gauge Company, Inc., Buffalo Grove, IL, USA) to determine the apparent thickness of each set. The untreated sheets had an apparent thickness of 40 ± 3 μm, while the acid-treated sheets had an apparent thickness of 24 ± 5 μm. The sheets were then weighed and measured to determine their apparent and areal densities. The apparent density of the untreated specimens was 0.40 ± 0.03 g m^{-3}, while the apparent density of the acid-treated specimens was 0.50 ± 0.03 g m^{-3}. The areal density of the untreated specimens was 16 ± 1 g m^{-2}, while the areal density of the acid-treated specimens was 12 ± 1 g m^{-2}. Variations in the measured densities are attributed to such factors as nanoscale voids among bulk CNTs [17], residual catalyst impurities encapsulated between sheet layers, or run-to-run process variations [18]. Unexposed, AO-exposed and temperature-cycled sheets from both sets were cut into 12.5 mm × 40 mm rectangular specimens for mechanical testing. A summary of the specimen types is presented in Table 1.

Table 2

Mechanical and electrical properties of the CNT specimens. Standard deviations with a (+) next to them indicate that they were calculated assuming the same spread as their respective unexposed specimens.
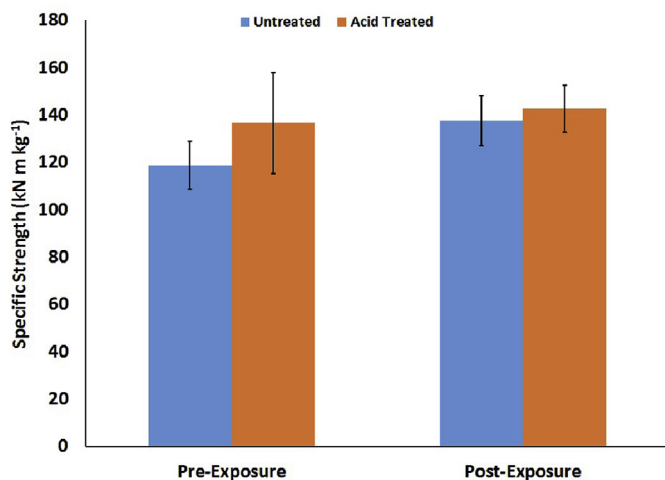
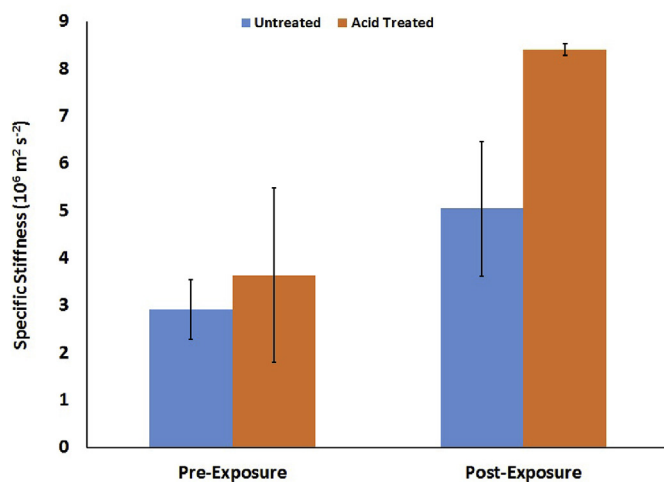| Specimen ID	Specific Strength (kN m kg^{-1})	Specific Stiffness (10^6 m^2 s^{-2})	Strain at Failure (%)	Apparent Conductivity (S m^{-1})	EMI Shielding (dB)
A-1	118.88 ± 10.10	2.92 ± 0.63	22 ± 4	23637 ± 2502	50.15 ± 0.66
A-2	114.76 ± 8.20	5.27 ± 1.46	13 ± 4	15354 ± 1251	49.79 ± 0.62$^+$
A-3	137.81 ± 10.55	5.05 ± 1.42	22 ± 4	40173 ± 2647	51.39 ± 0.59$^+$
B-1	136.64 ± 21.34	3.64 ± 1.84	29 ± 5	58948 ± 8873	60.90 ± 0.37
B-2	122.66 ± 17.23	7.43 ± 0.19	16 ± 3	21742 ± 1417	55.20 ± 0.64$^+$
B-3	142.60 ± 9.93	8.41 ± 0.12	17 ± 5	46020 ± 703	56.21 ± 0.54$^+$

(a)
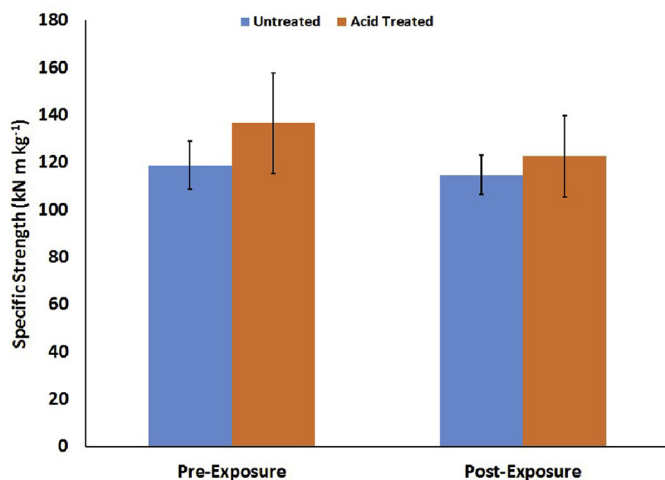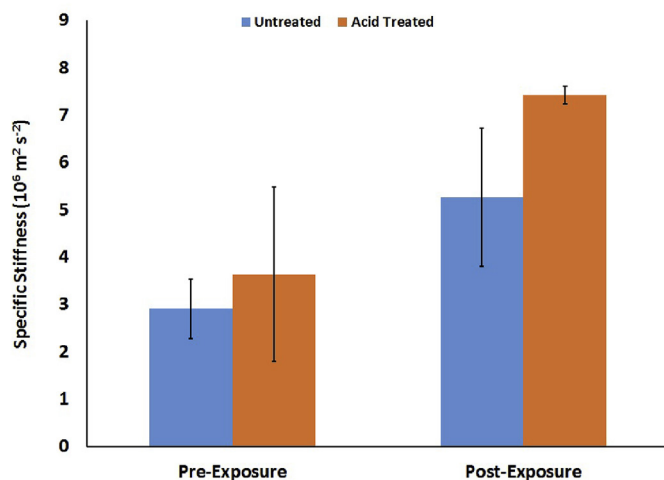
(b)

Fig. 5. Changes in the specific strengths of the CNT sheets after being exposed to AO (a) and thermal fatigue (b). Both the untreated and acid-treated specimens are presented. Neither exposure type significantly affected the specific strength.

2.2. Exposure to atomic oxygen

Two specimens were sent to Montana State University to undergo Hyperthermal AO exposure for a simulated three month period in LEO. They were held on a 76 mm × 76 mm sample mount where the sheets were suspended above an aluminum plate as shown in Fig. 2. The specimens were exposed to AO using a directed beam containing O and O$_2$ in an O/O$_2$ mole ratio of three or greater with normal incidence exposure on the plate. The specimens remained at room temperature during

(a)

(b)

Fig. 6. Changes in the specific stiffness of the CNT sheets after being exposed to AO (a) and thermal fatigue (b). Both the untreated and acid-treated specimens are presented. Both exposure types significantly increased the specific stiffness.

exposure in an oil-free vacuum chamber with a base pressure $<10^{-6}$ torr. The directed beam pulsed at 2 Hz with an approximate oxygen atom flux of 2×10^{15} atoms cm^{-2} pulse^{-1}. The oxygen atom flux is determined by parameters including altitude, orbital inclination, solar activity, and time of day. The nominal range of flux is typically 10^{14}-10^{15} atoms cm^{-2} s^{-1} [8]. O-atom fluence was nominal at 2×10^{20} atoms cm^{-2}, which was based on the erosion depth of a Kapton H sample that had an assumed erosion yield of 3.00×10^{-24} cm^{-3} O-atom^{-1}. The O-atom translational energy was nominal at 5 eV with a full width at half of the maximum energy with an approximate 1.5 eV energy distribution. The O$_2$
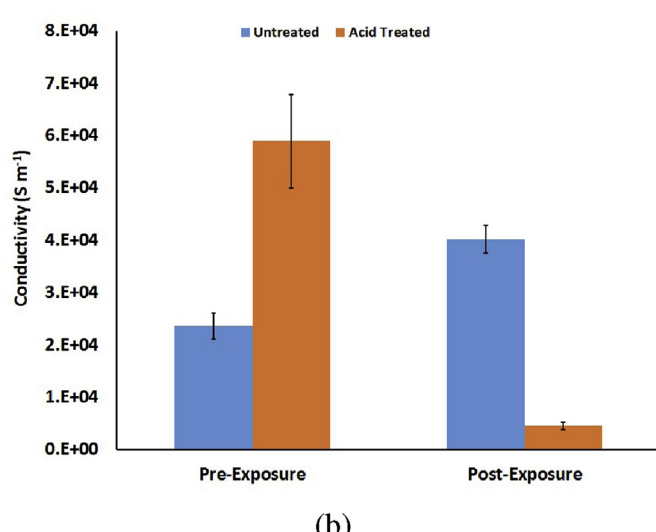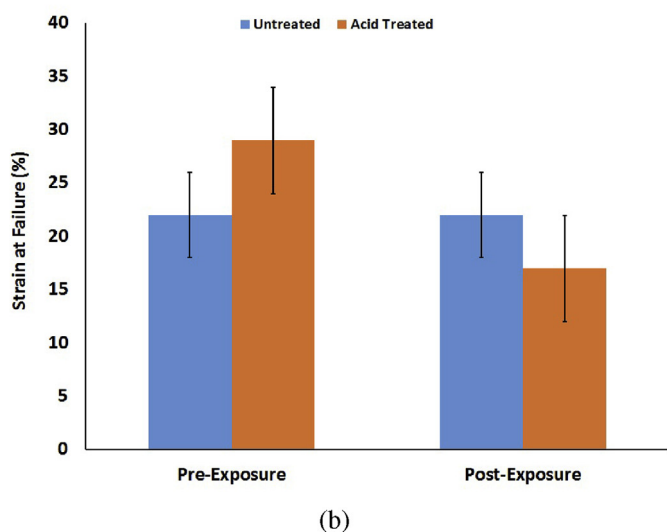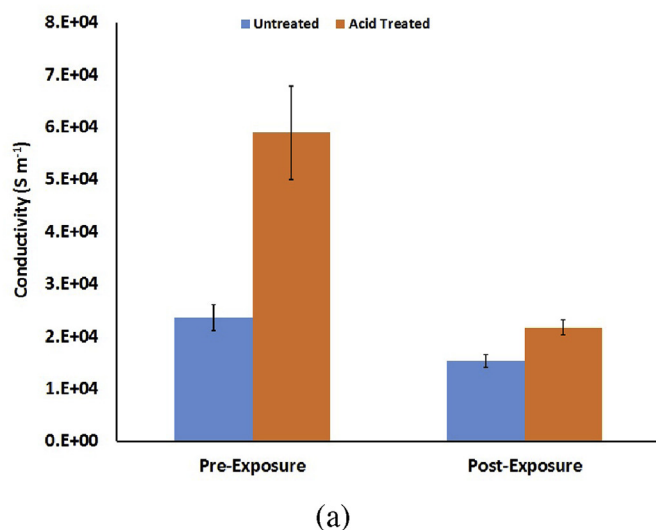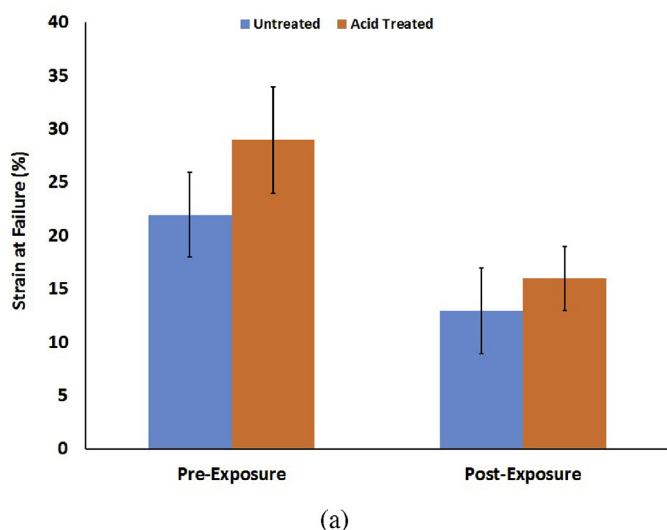
(a)

(b)

Fig. 7. Changes in the strain at failure of the CNT sheets after being exposed to AO (a) and thermal fatigue (b). Both the untreated and acid-treated specimens are presented. Both exposure types significantly decreased the strain at failure.

translational energy was nominally 8.8 eV, and the full width at half maximum in energy distribution was approximately 3.0 eV.

2.3. Thermal fatigue

Thermal fatigue testing was performed using an FTS Thermojet ES (SP Industries, Inc., Warminster, PA, USA) to simulate temperature cycles experienced in LEO. The specimens were prepared and tested using the same apparatus shown in Fig. 2. Temperatures were cycled between −60 °C and 120 °C at an average rate of ±18 °C min^{-1}. The air flow rate was 9 L min^{-1}, and the test was performed in a standard room-temperature laboratory atmosphere. 1440 cycles were conducted. This is equivalent to three months of exposure in LEO assuming that the orbit period of the spacecraft is 90 min. The first three cycles are presented in Fig. 3.

2.4. Mechanical testing

Mechanical testing was performed with an MTS Tytron 250 bench-type test machine (MTS, Eden Prarie, MN, USA) with a 50 N load cell. The specimens were glued between two thin pieces of fiberglass with epoxy resin to protect the ends from premature failure at the grips. The

(a)

(b)

Fig. 8. Changes in the apparent conductivity of the CNT sheets after being exposed to AO (a) and thermal fatigue (b). Both the untreated and acid-treated specimens are presented. Both exposure types significantly decreased the apparent conductivity.

tensile test was displacement controlled and was performed at a displacement rate of 2 mm min^{-1}. The system recorded the time, applied force, and displacement data measured during the experiment, and these measurements were used to calculate the engineering stress and strain. Three of the four specimens from each specimen type were used for tensile testing, resulting in 18 tested samples.

2.5. Electrical conductivity measurement

A Keithley 2400 source meter (Keithley Instruments, Inc., Cleveland, OH, USA) was used to measure the electrical resistivity at a maximum current detection of 10 mA. Since the sheets' thicknesses were much smaller than their respective lengths or widths and the specimen is highly conductive, the four-point probe method was used to measure the apparent conductivity. A description of this method is available in the literature [19]. The conductivity was measured using the same setup previously utilized by the authors [15]. Due to the damage that this test setup can cause the specimens, only one specimen from each test case was studied. However, the conductivity was measured across multiple areas on the specimens to generate statistical data.
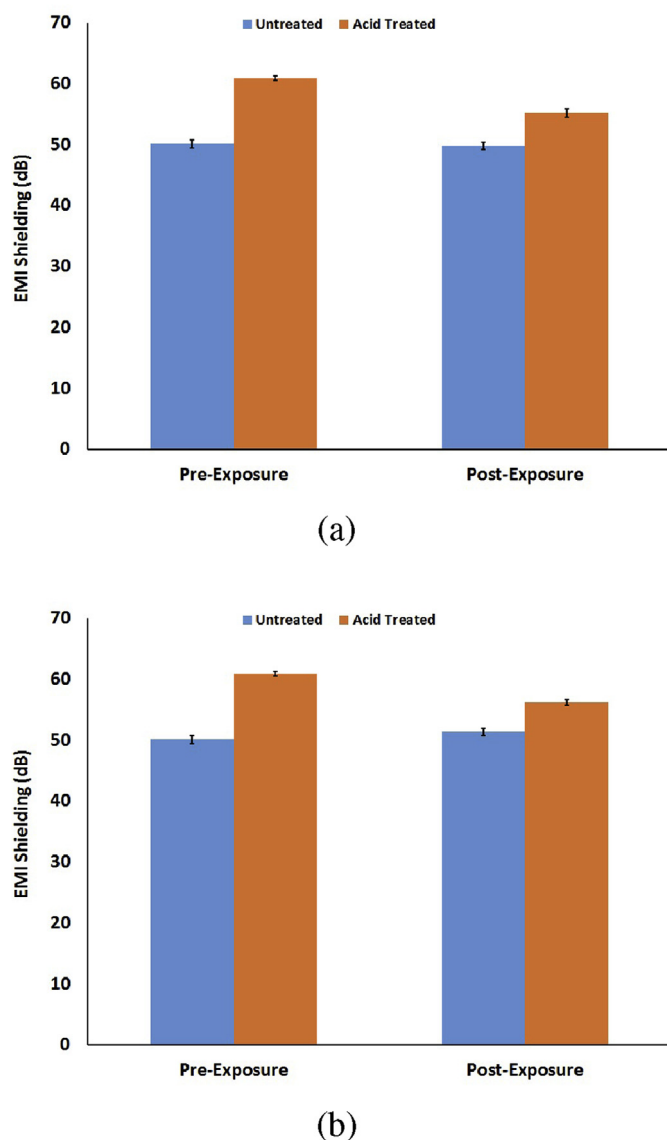
(a)

(b)

Fig. 9. Changes in the range of EMI shielding of the CNT sheets after being exposed to AO (a) and thermal fatigue (b). Both the untreated and acid-treated specimens are presented. The sheets' EMI shielding effectiveness is not affected by either exposure type.

2.6. EMI shielding

The sheets' EMI shielding efficiency was determined with a Keysight E8563 PNA Microwave Network Analyzer (Keysight Technologies, Santa Rosa, CA, USA). Frequencies ranging from 8.2 GHz to 12.4 GHz were produced and transmitted through the specimens. Signals were sent in both directions through the material to verify directional consistency in shielding properties. The signal that passed through the specimen as well as the signal reflected from the material surface were measured in both directions. This resulted in four recorded signal readings.

2.7. Scanning electron microscopy

Micrographs of the specimens were collected with an FEI XL40 Sirion field-emission source SEM (Thermo Fisher Scientific, Waltham, MA, USA). The source beam had an accelerating voltage of 5 kV. Elemental analysis was performed separately in a Quanta 450 SEM (Thermo Fisher Scientific, Waltham, MA, USA) using an EDAX EDS detector (Ametek Materials Analysis Division, Mahwah, NJ, USA). The accelerating voltage used to collect EDS data was 5 kV.

3. Results and discussion

3.1. Monotonic tensile properties

Specimens from each set were loaded to failure to determine the sheets' specific strengths, specific stiffnesses, and strains at failure. Example stress-strain data from each specimen set is presented in Fig. 4, and the calculated values are presented in Table 2. The specific strength and stiffness values are presented to allow for direct comparisons between the treated and untreated specimens as well as other materials such as steel. The specimens exhibited the same surface CNT alignment and failure behavior previously reported by the authors [15]. The acid treatment did not affect either of these properties.

The specific strengths of the specimens subjected to AO exposure and thermal fatigue are presented in Fig. 5. The unexposed specimens are also presented as a baseline for comparison. Neither exposure type affected the specific strength by more than 10%. Although AO is known to be a destructive material, the insignificant change in the specific strength indicates that it only penetrates into the outer layers of the sheet. Unlike the specific strength, the specific stiffness was significantly increased by both exposure types. The stiffness data are presented in Fig. 6. The AO specimens' specific stiffness increased by more than 70% (Fig. 6a), while thermal cycling increased the stiffness by 55% for the untreated specimen and 79% for the acid-treated specimen (Fig. 6b). This suggests that neither exposure type inhibits CNT alignment, which was reported to increase the stiffness of CNT-based materials [20]. Fig. 7 presents the final strain at failure. The amount of strain at failure decreased in all cases. This is expected because of the increased stiffness exhibited by the specimens.

3.2. Electrical properties

The electrical conductivities and EMI shielding properties of the baseline, AO-exposed and thermal fatigue specimens are also presented in Table 2. Due to the limited number of specimens available for EMI shielding tests, the standard deviations of the exposed specimens were calculated assuming the same spread as the unexposed specimens. The electrical conductivity data are presented in Fig. 8, while the EMI shielding data are presented in Fig. 9. AO exposure reduced the apparent conductivity by more than 30% for both exposure types (see Fig. 8a). The destructive nature of the AO exposure possibly damaged the CNT fibrous network as well as the individual CNTs, which in turn reduced the in-plane conductivity of the sheet. Thermal fatigue reduced the conductivity of the acid-treated specimens by 26%, but did not significantly affect the untreated conductivity (Fig. 8b). The acid in the sheets likely liquefied and recondensed during thermal cycling. This process may have promoted greater infiltration of acid between individual CNTs. This infiltration would reduce the number of electrical connections in the sheet network, which would reduce the overall conductivity of the sheet. In addition, expansion and contraction of CNTs may have separated CNTs and promoted acid infiltration into these gaps. Since the untreated specimens only contain CNTs and iron catalyst, these gaps were closed upon contraction and bonding between CNTs was recovered. The EMI shielding data presented in Fig. 9 indicates neither exposure type affected the sheets' EMI shielding effectiveness. The sheets' shielding effectiveness must be only due to the presence of CNTs and be unaffected by other factors such as cross-linking or in-plane alignment.

3.3. Microscopy and chemical analysis

Scanning electron micrographs of specimens collected before and after AO exposure are presented in Fig. 10. The untreated specimen presented in Fig. 10a contains the same network of CNTs and iron catalyst previously seen with this type of material [15], while the CNTs of
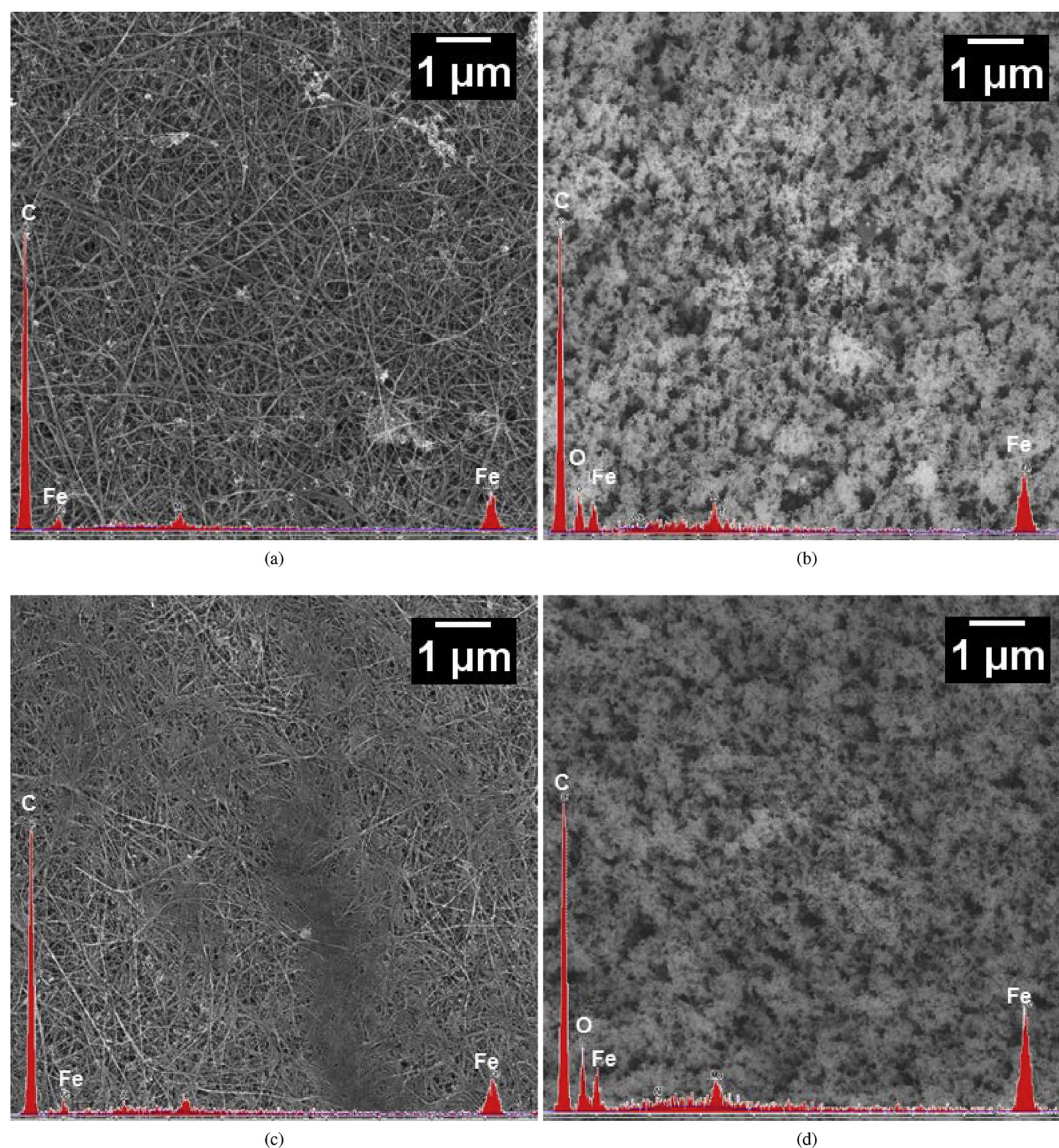
Fig. 10. Micrographs of the untreated (a–b) and acid-treated (c–d) specimens. The images in (a) and (c) were taken prior to AO exposure, while the images in (b) and (d) were taken after AO exposure. Each specimen's EDS data are also included.

the acid-treated specimen found in Fig. 10c are more agglomerated. In contrast, the specimens found in Fig. 10b and d appears to be more pitted and "carpet like," and the CNT fibril network has been broken. The observed erosion pattern matches previous observations of materials studied on the STS-5 mission [21]. The authors assume that this damage only occurred at the outermost layer and did not penetrate into the CNT sheet based on their previous research with CNT yarns [22]. Scanning electron micrographs of specimens subjected to thermal fatigue are presented in Fig. 11. There is no apparent change between the thermally cycled specimens and the pre-AO exposure specimens presented in Fig. 10. This indicates that thermal cycling did not significantly affect the microstructure of the CNT sheet.

EDS spectra are also presented in Fig. 10, while the corresponding data is presented in Table 3. The chemical compositions are presented by weight percent. Significant carbon (CNTs) and iron (excess catalyst) peaks were found in all specimens. Trace amounts of other materials were measured and recorded in the "Other" section in Table 3. The EDS spectra of the AO-exposed specimens also contain significant oxygen peaks. These peaks verify that AO exposure causes the CNT sheet to oxidize and are in agreement with results of AO exposure on other carbon-based materials reported by Zhao et al. [10]. The increase in the

weight percent of iron and trace materials is caused by erosion of the surface layer, which causes more residual catalyst and trace materials to be exposed. An example of this is presented in Fig. 12.

3.4. Statistical analysis

The significance of the changes in mechanical and electrical properties of the specimens was determined using a two-tailed t-test. Unequal variance was assumed for all results. An value of 0.05 was used to determine statistical significance. Table 4 presents the percent changes of the studied properties when compared to their respective baseline material. The table has been color coded to show which changes the t-test determined were statistically significant, possibly statistically significant, or not statistically significant. From this table, it is obvious that the changes in specific strength were not statistically significant for any specimen. In addition, the acid-treated specimens were more significantly affected by both exposure types than the untreated specimens. Given the limited number of samples tested, further exposure testing is necessary to assess the statistical significance of the observed changes in the material properties of untreated sheets.
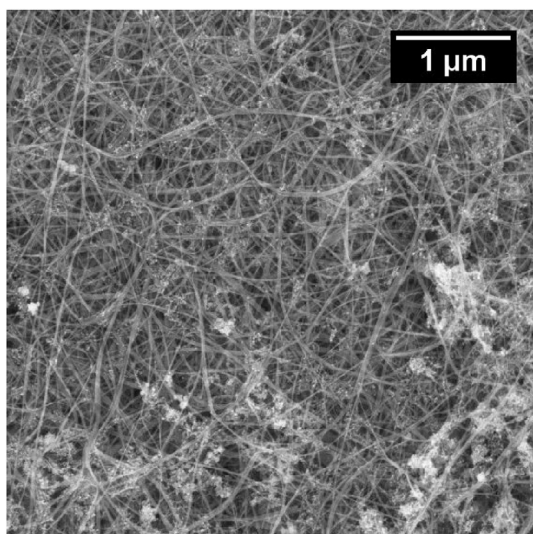
(a)
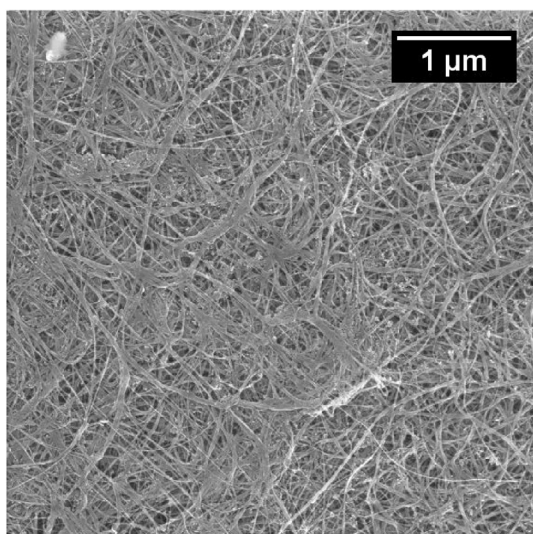
(b)

Fig. 11. Micrographs of the untreated (a) and acid-treated(b) specimens after being exposed to thermal fatigue. The specimens' surface morphology does not change as a result of thermal fatigue (compare with the pre-exposed specimens presented in Fig. 10).

Table 3
Chemical composition of the CNT sheets before and after AO exposure.

Element	Untreated		Acid Treated	
	Pre-AO (% Weight)	Post-AO (% Weight)	Pre-AO (% Weight)	Post-AO (% Weight)
C	86.01	73.12	83.73	70.3
Fe	11.01	12.66	12.6	15.24
O	0.00	9.27	0.00	7.81
Other	2.98	4.95	3.68	6.65

4. Conclusions

The mechanical and electrical properties of CNT sheet exposed to AO and thermal cycling were measured and analyzed. The specific stiffness of all of the specimens did not change in a statistically significant way. The specific stiffness increased due to both exposure types, while the strain at failure decreased in all cases. The conductivity of the specimens
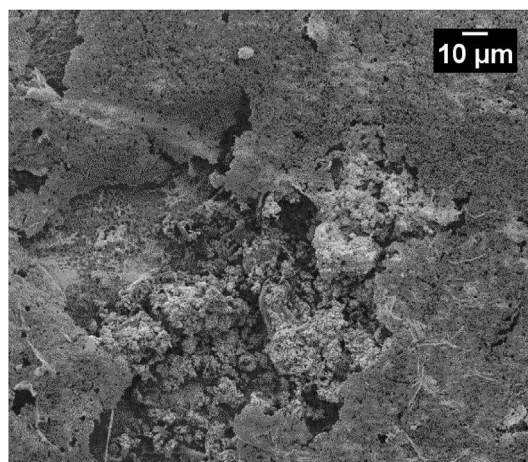

Fig. 12. CNT sheet after being exposed to AO. The light grey area is a cluster of exposed iron catalyst and trace materials exposed by AO-induced erosion.

Table 4
Results of t-tests performed to determine which material properties were significantly affected by the different exposure types.

Property	Untreated		Acid-Treated	
	AO	Thermal	AO	Thermal
Specific Strength	-10%	+8%	<+1%	+8%
Specific Stiffness	+74%	+55%	+71%	+79%
Failure Strain	-40%	-6%	-39%	-33%
Apparent Conductivity	-32%	-8%	-35%	-26%
EMI Shielding	<-1%	+3%	-2%	-1%

Legend			
t< 0.05	t< 0.10	t< 0.15	t> 0.15

decreased after both types of exposure, while the EMI shielding effectiveness was not affected by the exposure. The microstructure was analyzed using multiple techniques to determine if AO exposure or thermal cycling caused any significant microstructural changes. AO exposure caused the CNT sheets to erode, but thermal fatigue had no effect on the specimens. EDS analysis confirmed that AO exposure causes the surface of the CNT sheets to oxidize, and the acid treatment does not inhibit oxidation. The results of the experiments show that these materials could effectively serve as EMI shields or be implemented into load-bearing structures. However, they should not be used as conductive materials unless they are properly shielded from the harsh atmosphere of space.

References

[1] J.-P. Salvetat, J.-M. Bonard, N. Thomson, A. Kulik, L. Forró, W. Benoit, L. Zuppiroli, Mechanical properties of carbon nanotubes, Appl. Phys. A 69 (3) (1999) 255–260, https://doi.org/10.1007/s003390050999.

[2] R.H. Baughman, A.A. Zakhidov, W.A. de Heer, Carbon nanotubes–the route toward applications, Science 297 (5582) (2002) 787–792, https://doi.org/10.1126/science.1060928.

[3] M.H. Al-Saleh, W.H. Saadeh, U. Sundararaj, EMI shielding effectiveness of carbon based nanostructured polymeric materials: a comparative study, Carbon 60 (2013) 146–156, https://doi.org/10.1016/j.carbon.2013.04.008.

[4] J.C. Coopersmith, E. Davis, A strategic roadmap for commercializing low-cost beamed energy propulsion launch systems, in: AIAA SPACE, 2016, pp. 1–12, https://doi.org/10.2514/6.2016-5555, 2016.

[5] P.R. Jarosz, A. Shaukat, C.M. Schauerman, C.D. Cress, P.E. Kladitis, R.D. Ridgley, B.J. Landi, High-performance, lightweight coaxial cable from carbon nanotube conductors, ACS Appl. Mater. Interfaces 4 (2) (2012) 1103–1109, https://doi.org/10.1021/am201729g.

[6] I. Puchades, J.E. Rossi, C.D. Cress, E. Naglich, B.J. Landi, Carbon nanotube thin-film antennas, ACS Appl. Mater. Interfaces 8 (32) (2016) 20986–20992, https://doi.org/10.1021/acsami.6b05146.

[7] S. Rawal, J. Brantley, N. Karabudak, Development of carbon nanotube–based composite for spacecraft components, in: 2013 6th International Conference on Recent Advances in Space Technologies (RAST), 2013, pp. 13–19, https://doi.org/10.1109/RAST.2013.6581186.

[8] E. Grossman, I. Gouzman, Space environment effects on polymers in low earth orbit, Nucl. Instrum. Methods Phys. Res. Sect. B Beam Interact. Mater. Atoms 208 (2003) 48–57, https://doi.org/10.1016/S0168-583X(03)00640-2.

[9] R. Kiefer, R. Anderson, M.-H. Kim, S. Thibeault, Modified polymeric materials for durability in the atomic oxygen space environment, Nucl. Instrum. Methods Phys. Res., Sect. B: Beam Interact. Mater. Atoms 208 (2003) 300–302, https://doi.org/10.1016/S0168-583X(03)00665-7, ionizing Radiation and Polymers.

[10] X.-H. Zhao, Z.-G. Shen, Y.-S. Xing, S.-L. Ma, An experimental study of low earth orbit atomic oxygen and ultraviolet radiation effects on a spacecraft material – polytetrafluoroethylene, Polym. Degrad. Stab. 88 (2) (2005) 275–285, https://doi.org/10.1016/j.polymdegradstab.2004.11.002.

[11] K.-B. Shin, C.-G. Kim, C.-S. Hong, H.-H. Lee, Prediction of failure thermal cycles in graphite/epoxy composite materials under simulated low earth orbit environments, Compos. B Eng. 31 (3) (2000) 223–235, https://doi.org/10.1016/S1359-8368(99)00073-6.

[12] J.-H. Han, C.-G. Kim, Low earth orbit space environment simulation and its effects on graphite/epoxy composites, Compos. Struct. 72 (2) (2006) 218–226, https://doi.org/10.1016/j.compstruct.2004.11.007.

[13] J.-B. Moon, M.-G. Kim, C.-G. Kim, S. Bhowmik, Improvement of tensile properties of CFRP composites under LEO space environment by applying MWNTs and thin-ply, Compos. Appl. Sci. Manuf. 42 (6) (2011) 694–701, https://doi.org/10.1016/j.compositesa.2011.02.011.

[14] H. Misak, V. Sabelkin, S. Mall, P. Kladitis, Thermal fatigue and hypothermal atomic oxygen exposure behavior of carbon nanotube wire, Carbon 57 (2013) 42–49, https://doi.org/10.1016/j.carbon.2013.01.028.

[15] G.R. Cobb, R.P. O'Hara, R.A. Kemnitz, V.P. Sabelkin, B.M. Doane, Quantifying the effects of ultraviolet type C radiation on the mechanical and electrical properties of carbon nanotube sheet for space-based applications, Mater. Today Commun. 18 (2019) 7–13, https://doi.org/10.1016/j.mtcomm.2018.10.016.

[16] J.C. Fernández-Toribio, B. Alemán, Á. Ridruejo, J.J. Vilatela, Tensile properties of carbon nanotube fibres described by the fibrillar crystallite model, Carbon 133 (2018) 44–52, https://doi.org/10.1016/j.carbon.2018.03.006.

[17] H. Misak, S. Mall, Electrical conductivity, strength and microstructure of carbon nanotube multi-yarns, Mater. Des. 75 (2015) 76–84, https://doi.org/10.1016/j.matdes.2015.03.020.

[18] S.J. Park, A.J. Schmidt, M. Bedewy, A.J. Hart, Measurement of carbon nanotube microstructure relative density by optical attenuation and observation of size-dependent variations, Phys. Chem. Chem. Phys. 15 (27) (2013) 11511–11519, https://doi.org/10.1039/C3CP51415C.

[19] M.B. Heaney, Electrical conductivity and resistivity, in: J.G. Webster (Ed.), Electrical Measurement, Signal Processing, and Displays, CRC Press, 2003, pp. 7.1–7.14. Ch. 7.

[20] X. Wang, Z. Yong, Q. Li, P. Bradford, W. Liu, D. Tucker, W. Cai, H. Wang, F. Yuan, Y. Zhu, Ultrastrong, stiff and multifunctional carbon nanotube composites, Mater. Res. Lett. 1 (1) (2013) 19–25, https://doi.org/10.1080/21663831.2012.686586.

[21] L.J. Leger, J.T. Visentine, J.F. Kuminecz, Low earth orbit atomic oxygen effects on surfaces, in: AIAA 22nd Aerospace Sciences Meeting, 1984, pp. 1–8, https://doi.org/10.2514/6.1984-548.

[22] R.A. Kemnitz, G.R. Cobb, A.K. Singh, C.R. Hartsfield, Characterization of Simulated Low Earth Orbit Space Environment Effects on Acid-Spun Carbon Nanotube Yarns, Materials & Design, 2019, https://doi.org/10.1016/j.matdes.2019.108178, 108178.